Available online at www.sciencedirect.com

ScienceDirect

J Materiomics 2 (2016) 172–178

www.ceramsoc.com/en/

www.journals.elsevier.com/journal-of-materiomics/

Enhanced thermoelectric performance of MnTe *via* Cu doping with optimized carrier concentration

Yangyang Ren[1], Qinghui Jiang[1], Junyou Yang*, Yubo Luo, Dan Zhang, Yudong Cheng, Zhiwei Zhou

State Key Laboratory of Materials Processing and Die & Mould Technology, Huazhong University of Science and Technology, Wuhan 430074, China

Received 9 March 2016; revised 29 April 2016; accepted 4 May 2016
Available online 13 May 2016

Abstract

Polycrystalline $Mn_{1-x}Cu_xTe$ ($x = 0$, 0.025, 0.05, 0.075) thermoelectric materials were prepared by a combined method of melt-quenching and hot press. The effect of Cu doping on the electrical resistivity, band gap, the Seebeck coefficient and thermal conductivity was investigated. The power factors of the Cu-doped samples increase greatly due to the decrease of electrical resistivity and the higher Seebeck coefficient in high temperatures. In addition, the thermal conductivities of the Cu-doped samples also reduce due to the extra phonon scattering from the point defects introduced by Cu doping. As a result, the thermoelectric performance of MnTe is greatly enhanced, and a maximum *ZT* value of ~0.55 in the $Mn_{0.925}Cu_{0.075}Te$ sample at 773 K is achieved, which is 35% greater than that of the pristine MnTe sample.

Keywords: MnTe; Thermoelectric materials; Doping; Carrier concentration

1. Introduction

Thermoelectric (TE) materials have attracted much attention due to their ability to convert heat directly into electricity [1–3]. In general, the conversion efficiency of a TE device depends on the dimensionless figure of merit *ZT* of the TE materials employed, i.e., $ZT = S^2T/\rho\kappa$, where *S* is the Seebeck coefficient, ρ is the electrical resistivity, κ is the thermal conductivity and *T* is the absolute temperature. Therefore, effective TE materials should have a high power factor ($S^2\sigma$) as well as a low thermal conductivity (κ). However, it is challenging for researchers to decouple these parameters and achieve high *ZT* values due to the interdependent relationship between the electrical and thermal parameters [4]. Many efforts have been made to improve the *ZT* value of TE materials through two main approaches so far. One approach is to increase the power factor by carrier engineering [5] or band engineering [6], and the another is to reduce the lattice thermal conductivity *via* nano-inclusions [7] or point defects [8]. Consequently, some encouraging results have been achieved in some material systems, such as Bi_2Te_3-based [9], PbTe-based [10], $CoSb_3$-based [11], etc.

Chalcogenide MnTe compound [12] has a typical hexagonal NiAs crystal structure with a large indirect band gap of 1.27 eV and a relatively low hole concentration ($p = 10^{18}$ cm^{-3}) at room temperature. Recently, wide band gap semiconductors are frequently employed as potential TE materials due to their intrinsic large Seebeck coefficient and low thermal conductivity [13], which can work at a relatively high temperature. Thus, MnTe can be a potential candidate for middle-temperature thermoelectric application. Some studies have focused on the low-temperature electrical, magnetic and optical properties of MnTe compound [14–17], and MnTe has also been incorporated into PbTe, GeTe and SnTe thermoelectric materials [18–20] to improve their thermoelectric

* Corresponding author.
E-mail address: jyyang@mail.hust.edu.cn (J. Yang).
Peer review under responsibility of The Chinese Ceramic Society.
[1] These authors contributed equally to this work.

http://dx.doi.org/10.1016/j.jmat.2016.05.008

performance. However, less attention has been paid to its own intrinsic thermoelectric performance. More recently, Kim, et al. [21] prepared bulk non-stoichiometric MnTe materials by a melt-quenching plus spark plasma sintering method, and achieved a high Seebeck coefficient of over 600 μV/K at room temperature and a promising *ZT* value of ~0.41 in the $Mn_{0.51}Te_{0.49}$ sample at 773 K. In the light of the band structure of MnTe, the large Seebeck coefficient is closely related to the large band gap and the *p-d* overlap induced van Hove singularity in the electron density of states near the valence band edge [22]. Xie et al. [23] reported an enhanced TE performance in a sulfur doped MnTe in a low temperature range as a consequence of the increase of electrical properties and the decrease of thermal conductivity, however, the TE performance at a high temperature has no improvement at all. In general, the large electrical resistivity hinders the compound from achieving a high *ZT* value. Therefore, tuning its electrical properties is a key issue to improve the TE performance of the compound. Clearly, there are two possible doping sites in MnTe, i.e., the cation and anion sites. Some work on anion doping have already been tried, however, little work on cation doping in MnTe have ever been reported yet.

In this paper, Cu was doped into MnTe to substitute Mn cations for the improvement of its hole concentration and electrical properties. The samples of Cu-doped $Mn_{1-x}Cu_xTe$ (x = 0, 0.025, 0.05, 0.075) were prepared *via* a combined method of melt-quenching and hot press. The effect of Cu doping on the electrical and thermal transport properties the $Mn_{1-x}Cu_xTe$ samples was investigated.

2. Experimental

2.1. Preparation

Cu-doped $Mn_{1-x}Cu_xTe$ (x = 0, 0.025, 0.05, 0.075) ingots were prepared *via* a vacuum melting method. The powders of Mn (99.9%), Te (99.99%) and Cu (99.9%) were weighed and loaded into quartz tubes after mixing, then the quartz tubes were evacuated and sealed to ensure a vacuum atmosphere (10^{-3} Pa). The sealed quartz tubes were slowly heated up to 1273 K, held at this temperature for 2 days followed by water quenching. The obtained ingots were ground to fine powders in an agate mortar and reconsolidated by a hot press under an axial pressure of 120 MPa in a purified argon atmosphere at 923 K for 2 h. The relative density is above 95% for all the hot pressed samples.

2.2. Characterization

The structure and phase purity of samples were characterized by a powder X-ray diffraction (XRD) in a model X'Pert PRO diffractometer with Cu Kα radiation (λ = 0.15418 nm) (Philips Co. Ltd., the Netherlands). The fracture morphologies of the samples were observed by a model NanoSEM 450 field-emission scanning electron microscope (FSEM). The Seebeck coefficient and electrical resistivity were simultaneously measured using a model Namicro-III thermoelectric measurement system. Thermal conductivity (κ) is calculated according to $\kappa = DC_p\lambda$, where D is the density, which was determined by the Archimedes method, C_p is the specific heat capacity and the literature value of C_p [23] for MnTe compound was used for all the samples, and λ is the thermal diffusivity measured by a model LFA-427 laserflash diffusivity instrument (Netzsch Co. Ltd., Germany). The Hall measurements were accomplished by van der Pauw method in a model HMS 5500 Hall effect measurement system.

3. Results and discussion

3.1. Phase identification

Fig. 1a shows the X-ray diffraction patterns (XRD) of the $Mn_{1-x}Cu_xTe$ (x = 0, 0.025, 0.05, 0.075, 0.1) samples. For x from 0 to 0.075, all the XRD peaks can be well indexed as a hexagonal MnTe phase (space group, P63/mmc), and no peak of secondary phase is detected, indicating that single phase MnTe-based compounds can be obtained within the composition range of doping. However, $MnTe_2$ impurity phase was clearly found in $Mn_{0.9}Cu_{0.1}Te$ sample, which is negative to the electrical transport property of MnTe. In Fig. 1b, the XRD peaks shift toward a low angle direction due to the larger ionic radius of Cu^+ (77 pm) compared to Mn^{2+} (66 pm). This shift further confirms that Cu^+ has substituted the Mn^{2+} of the MnTe lattice. The lattice parameters of the samples were a = 4.1438, c = 6.7039; a = 4.1448, c = 6.7048; a = 4.1459, c = 6.7058; a = 4.1468, c = 6.7075; a = 4.1446, c = 6.7045, respectively. This increased lattice parameters are consistent with the shift of the XRD peaks.

Fig. 2 shows the SEM images of $Mn_{1-x}Cu_xTe$ (x = 0, 0.025, 0.05, 0.075) samples. Clearly, there is no evident difference among the hot-pressed samples. In addition, no crack and pore appear in the samples, indicating that they are a dense ploy-crystalline microstructure.

3.2. Electrical properties

Fig. 3a shows the temperature dependence of the electrical resistivity (ρ) of $Mn_{1-x}Cu_xTe$ (x = 0, 0.025, 0.05, 0.075) samples. The electrical resistivity of all samples decreases with increasing the temperature generally except an unconspicuous peak at 323 K. This characteristic should be attributed to the transition from antiferromagnetism to paramagnetism of MnTe at the Neel temperature [12]. The Seebeck coefficient (see Fig. 5a) and thermal conductivity (see Fig. 6a) also have such a characteristic at the same temperature. The ρ of $Mn_{1-x}Cu_xTe$ compounds exhibits a decrease within the exhaustion range from room temperature to 523 K, and it decreases rapidly with increasing the temperature due to the intrinsic excitation [23]. Besides, the ρ of all the samples decreases distinctly with increasing Cu doping content in the whole measured temperature range. Assuming a single parabolic band conduction process at 300 K, we estimated the carrier concentration (n) from the formula $n = 1/eR_H$, where e is the electronic charge. The measured carrier concentrations are ~6.8 × 10^{18} cm^{-3},

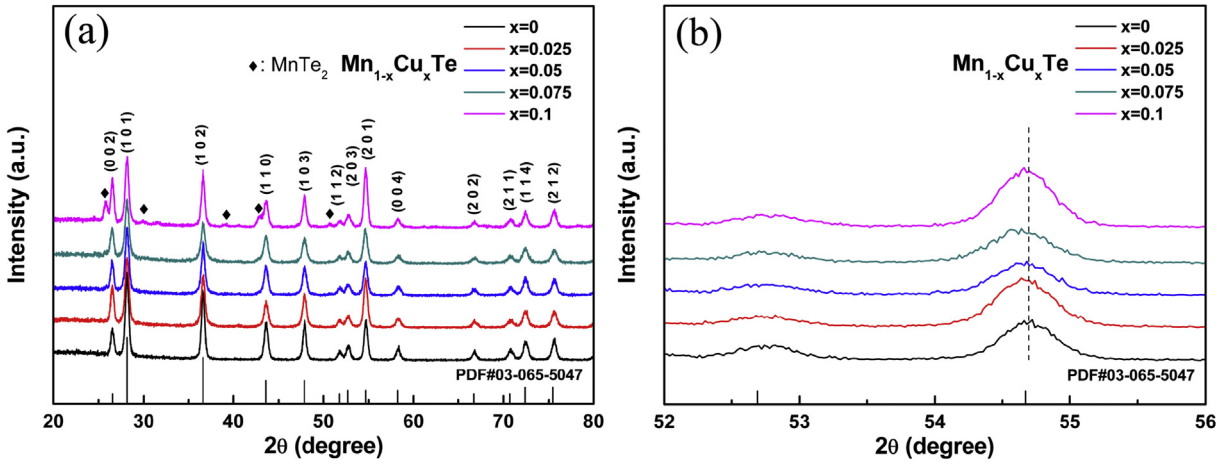

Fig. 1. (a) XRD patterns of $Mn_{1-x}Cu_xTe$ samples with different Cu doping content. (b) high angle XRD peak position comparison of the samples.

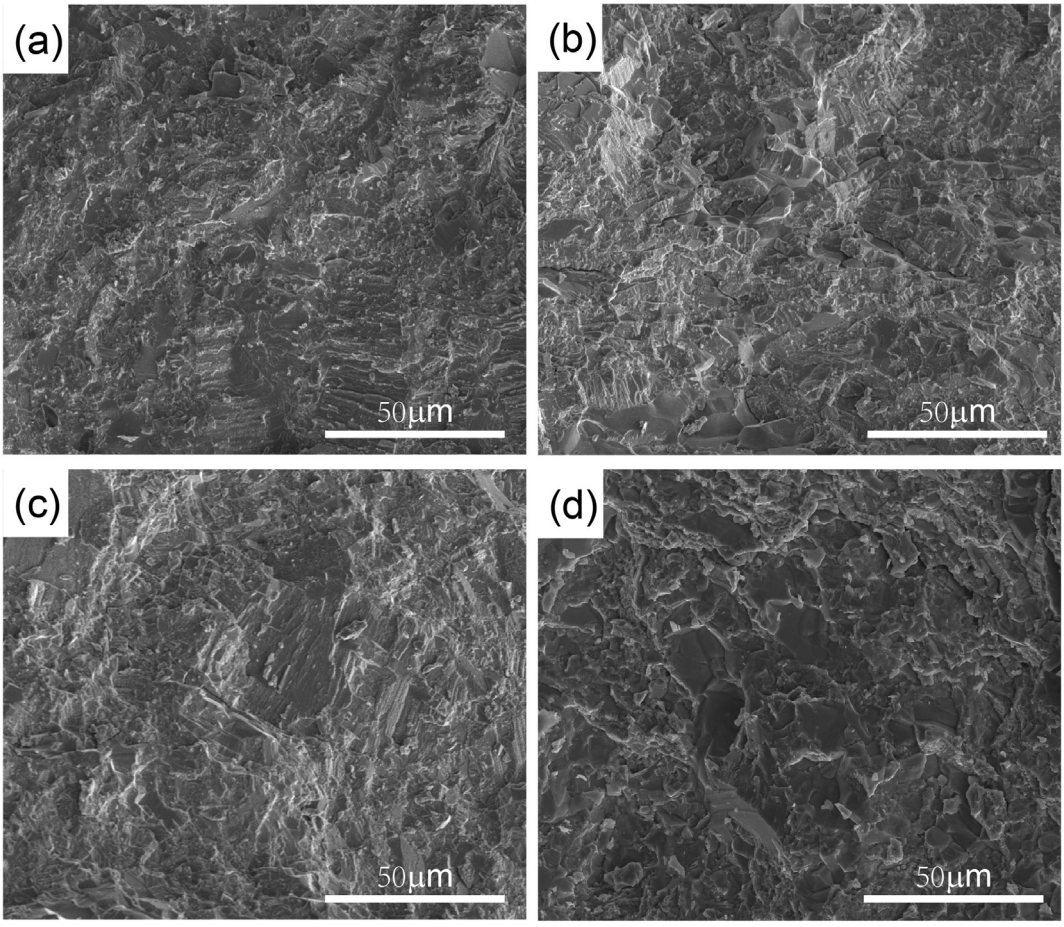

Fig. 2. SEM images of the samples with different contents of Cu doping (a) MnTe, (b) $Mn_{0.975}Cu_{0.025}Te$, (c) $Mn_{0.95}Cu_{0.05}Te$, (d) $Mn_{0.925}Cu_{0.075}Te$.

~1.7×10^{19} cm^{-3}, ~5.2×10^{19} cm^{-3}, and ~1.8×10^{20} cm^{-3} for the pristine MnTe, $Mn_{0.975}Cu_{0.025}Te$, $Mn_{0.95}Cu_{0.05}Te$, and $Mn_{0.925}Cu_{0.075}Te$ samples, respectively (see Table 1). Clearly, the carrier concentration increases rapidly with increasing Cu doping content, while the μ decreases due to the impurity scattering by dopants (see Fig. 3b). Thus, this decrease in electrical resistivity should be attributed to the increased carrier concentration by Cu doping, despite of the slight decrease in Hall mobility.

To further investigate the influence of Cu doping, the band gap was estimated from the slop of lnρ *vs*.1000/T curve (see Fig. 4a) according to the Arrhenius formula:

$$\rho = \rho_0 \exp\left(E_g/2k_BT\right) \quad (1)$$

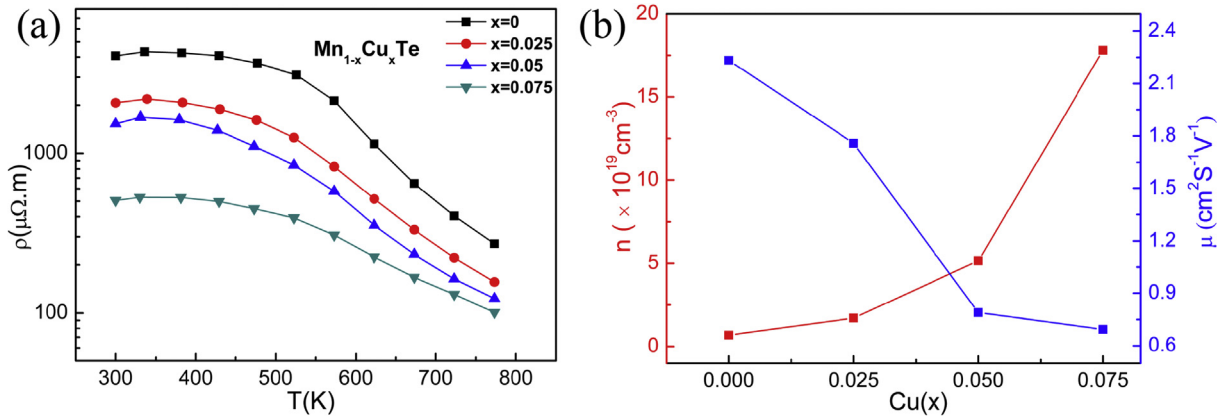

Fig. 3. (a) Temperature-dependent electrical resistivity (ρ) of $Mn_{1-x}Cu_xTe$ samples, (b) carrier concentration (n) and carrier mobility (μ) at room temperature with respect to Cu doping concentration (x) in $Mn_{1-x}Cu_xTe$ samples.

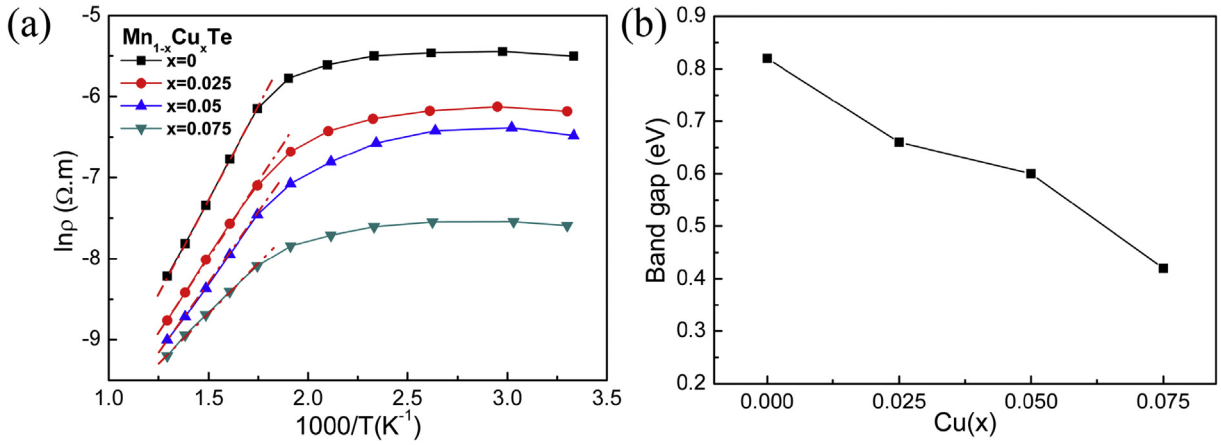

Fig. 4. (a) lnρ *vs.* 1000/T plot, (b) the calculated intrinsic band gap of $Mn_{1-x}Cu_xTe$(x = 0, 0.025, 0.05, 0.075).

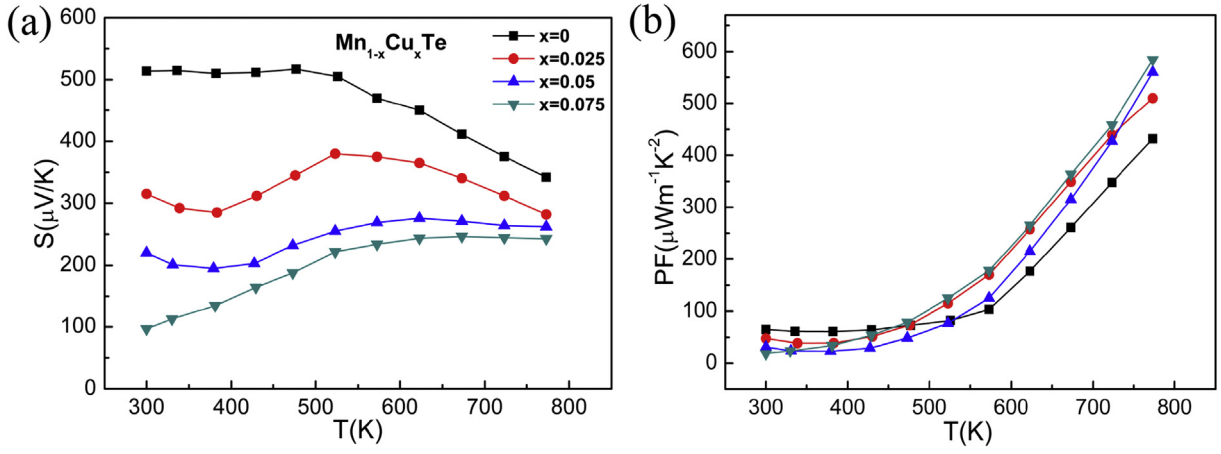

Fig. 5. (a) and (b) Temperature-dependent Seebeck coefficient (S) and power factor (σS^2), respectively.

where ρ is the electrical resistivity, and ρ_0 is a constant. The calculated intrinsic band gap values are 0.82, 0.66, 0.6 and 0.42 eV for the pristine MnTe, $Mn_{0.975}Cu_{0.025}Te$, $Mn_{0.95}Cu_{0.05}Te$, and $Mn_{0.925}Cu_{0.075}Te$ samples, respectively (see Fig. 4b). In which, the estimated band gap value of the pristine MnTe is similar to the theoretical result (0.8 eV) [24]. It can thus be concluded that the band gap of the samples narrows with increasing Cu content. This is consistent with the increase in carrier concentration and electrical conductivity.

Fig. 5a shows the temperature-dependent Seebeck coefficient of $Mn_{1-x}Cu_xTe$ (x = 0, 0.025, 0.05, 0.075) samples. At 300 K, the room-temperature Seebeck coefficient (S) of the

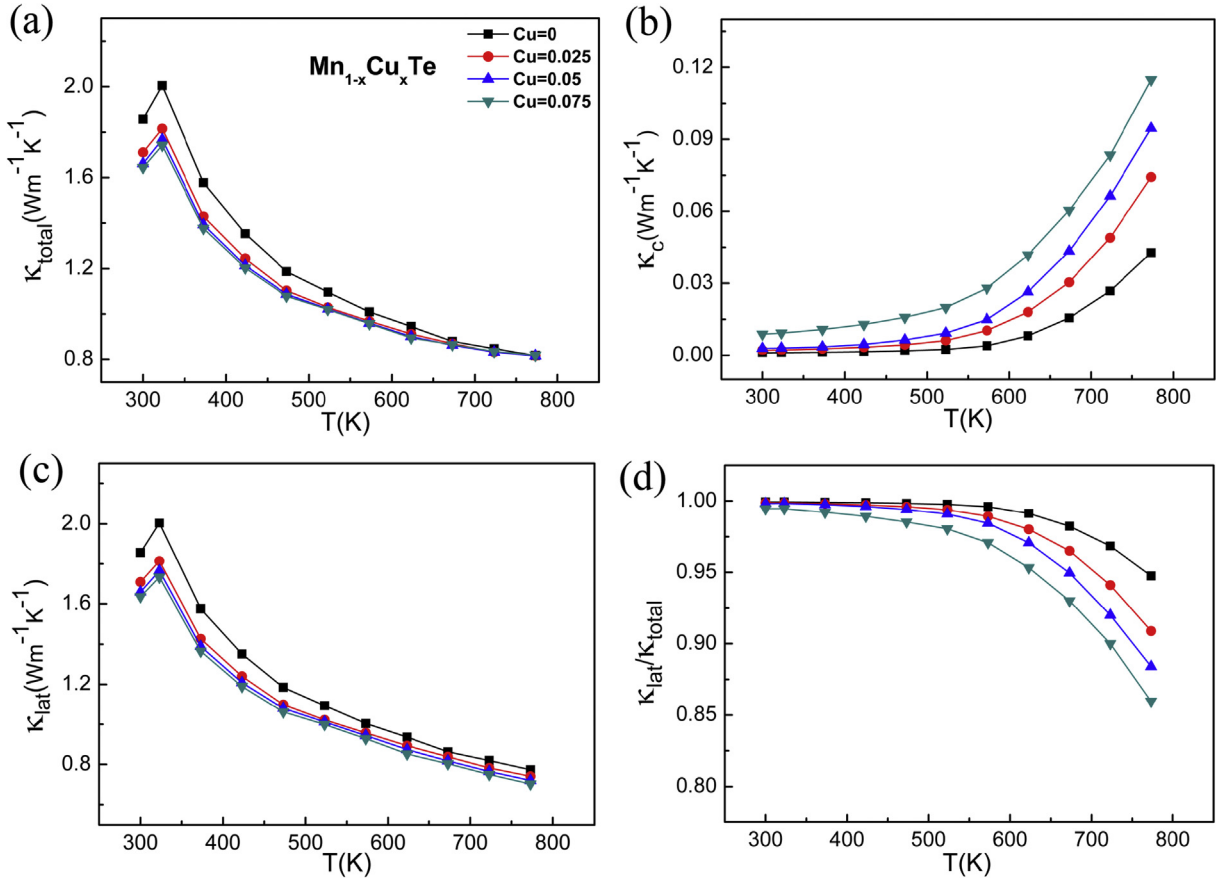

Fig. 6. Temperature-dependent (a) total thermal conductivity (κ_{total}), (b) carrier thermal conductivity (κ_c), (c) lattice thermal conductivity (κ_{lat}) and (d) $\kappa_{lat}/\kappa_{total}$ of the $Mn_{1-x}Cu_xTe$ ($x = 0$, 0.025, 0.05, 0.075) samples.

Table 1
Carrier concentration n_h, effect mass m^* of all the samples at room temperature.

Sample	n_h (10^{19} cm^{-3})	$m^*(m_0)$
MnTe	0.68	5.58
$Mn_{0.975}Cu_{0.025}Te$	1.71	2.38
$Mn_{0.95}Cu_{0.05}Te$	5.15	2.1
$Mn_{0.925}Cu_{0.075}Te$	17.8	1.45

pristine MnTe is 513.9 μV/K, and it decreases dramatically after doping Cu into Mn sites, displaying a similar trend with the electrical resistivity. In addition, the S for all the samples reduces with the increase of temperature at a high temperature, and the temperature factor of the S reduces gradually with the content of Cu. When the point defect is the top change in the samples with different contents of Cu, it should also be the main effect on the S for the samples. Assuming a single parabolic band model with acoustic phonon scattering for nondegenerate semiconductor, we estimate the effective mass m^* according to the following equation (2) using the measured S and Hall carrier concentrations (n):

$$S = \frac{k_B}{e}\left\{2 + \lambda + \ln\left[\frac{2(2\pi m^* k_B T/h^2)^{3/2}}{n}\right]\right\} \quad (2)$$

where m^* is the effective mass of carrier, e is the electronic charge, k_B is the Boltzmann constant, h is the Planck constant, and λ is the scattering parameter [23]. Considering $\lambda = 0$, 2 for the acoustic phonon scattering and ionized impurity scattering, respectively. m^* is calculated when $\lambda = 0$ and the acoustic phonon scattering is the dominant scattering mechanism in MnTe compound. The calculated m^* for the pristine, $Mn_{0.975}Cu_{0.025}Te$, $Mn_{0.95}Cu_{0.05}Te$, and $Mn_{0.925}Cu_{0.075}Te$ samples are $5.58m_0$, $2.38m_0$, $2.1m_0$ and $1.45m_0$, respectively (see Table 1). Therefore, the Seebeck coefficient of the doped samples is greatly lower than that of the undoped MnTe as a consequence of the increase in carrier concentration and the decrease in effective mass m^*.

Fig. 5b shows the temperature dependence of the power factor of $Mn_{1-x}Cu_xTe$ ($x = 0$, 0.025, 0.05, 0.075) samples. Typically, at room temperature, the power factor value for MnTe is 64.8 μW m^{-1} K^{-2}, which increases to a maximum of 431.7 μW m^{-1}K^{-2} at 773 K. With the increase of the Cu content, the power factor decreases from 64.8 μW m^{-1} K^{-2} for the pristine MnTe to 18.4 μW m^{-1} K^{-2} for $Mn_{0.925}Cu_{0.075}Te$ at room temperature, mainly due to the great decrease of the Seebeck coefficient. After 500 K, the power factor values for the doped samples exceed that of the pristine MnTe because of the increased electrical conductivity, then reach a maximum at 773 K. The power factor of

$Mn_{0.925}Cu_{0.075}Te$ becomes the maximum of 584.2 μW $m^{-1}K^{-2}$ at 773 K due to the decrease of the electrical resistivity and the relative high Seebeck coefficient at elevated temperature, which is 35.3% greater than that of the un-doped MnTe sample.

3.3. Thermal transport properties

Fig. 6a shows the total thermal conductivity (κ_{total}) of all $Mn_{1-x}Cu_xTe$ ($x = 0, 0.025, 0.05, 0.075$) samples. The κ_{total} of $Mn_{1-x}Cu_xTe$ samples generally decreases with increasing temperature except the transition point at 320 K. It is seen that the Cu-doped samples have lower κ_{total} than the pristine MnTe when the temperature is lower than 673 K, and the influence of Cu doping on the κ_{total} becomes slight at a high temperature. Generally, the κ_{total} consists of two parts, i.e., the lattice thermal conductivity (κ_{lat}) and the carrier thermal conductivity (κ_c). The κ_c was calculated using the Wiedemann-Franz law, $\kappa_c = L\sigma T$, where L is the Lorenz number, σ is the electrical conductivity and T is the absolute temperature. Here, when $L = 1.5 \times 10^{-8}$ V^2 K^{-2}, this value is usually suitable for nondegenerate semiconductors [25]. Thus, the temperature-dependent κ_{lat} values can be obtained by subtracting the κ_c from the κ_{total}. In Fig. 6b, the κ_c of the $Mn_{1-x}Cu_xTe$ samples increases largely with the increase of Cu doping content over the whole temperature range due to the enhanced electrical conductivity of samples. The κ_{lat} in Fig. 6c shows a slight decrease with increasing Cu doping concentration. This decrease in κ_{lat} can be ascribed to the extra point defects scattering for phonons, which is due to the mass fluctuation and strain field fluctuation by the substitution of Mn by Cu. In this case, we can conclude that the Cu doping has a slight effect on the κ_{total} at a high temperature due to the sharply increase in the κ_c of the Cu doped samples (see Fig. 6b). In addition, Xie, et al. [23] also reported that the bipolar effect could be an important factor.

Fig. 6d shows the calculated ratio of κ_{lat} in κ_{total} for all the $Mn_{1-x}Cu_xTe$ samples. Clearly, the $\kappa_{lat}/\kappa_{total}$ of the pristine MnTe sample decreases with increasing temperature, but it is greater than 90% over the whole temperature range. Moreover, the $\kappa_{lat}/\kappa_{total}$ of Cu-doped samples is lower than that of pristine MnTe sample due to the significantly enhanced electrical conductivity, but it can remain above 85% over the entire temperature range. Consequently, the κ_{total} in $Mn_{1-x}Cu_xTe$ system is mainly dominated by κ_{lat}, which conducts heat through lattice vibrations.

3.4. The dimensionless figure of merit ZT

Fig. 7 shows the dimensionless thermoelectric figure of merit (ZT) of the $Mn_{1-x}Cu_xTe$ ($x = 0, 0.025, 0.05, 0.075$) samples. Clearly, the ZT value of all the samples monotonously increases with the increase of temperature. Note that the ZT values of the Cu-doped samples are greater than that of the undoped MnTe due to the remarkably decreased electrical resistivity and slightly suppressed thermal conductivity as aforementioned, and the maximum ZT value of 0.55 at 773 K is achieved in the $Mn_{0.925}Cu_{0.075}Te$ sample, which is approximately 35% greater than that of the pristine MnTe sample.

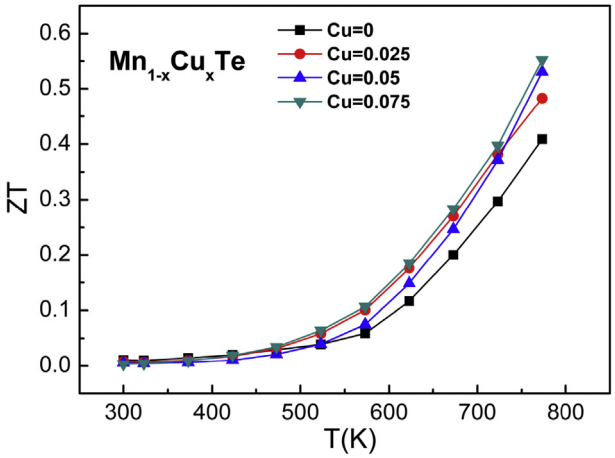

Fig. 7. Temperature-dependent thermoelectric figure of merit (ZT) of the $Mn_{1-x}Cu_xTe$.

4. Conclusions

A series of p-type Cu-doped $Mn_{1-x}Cu_xTe$ ($x = 0, 0.025, 0.05, 0.075$) samples were prepared by a combined method of melt-quenching and hot press. The band gap of $Mn_{1-x}Cu_xTe$ samples decreased correspondingly, and the electrical conductivity and power factor of the $Mn_{1-x}Cu_xTe$ samples increased with increasing the Cu doping concentration due to the increase of carrier concentration. In addition, the thermal conductivity was reduced due to the intensive scattering of phonons by the extra point defects introduced by Cu doping. As a consequence, a maximum ZT value of ~0.55 was obtained in the $Mn_{0.925}Cu_{0.075}Te$ sample at 773 K, which was approximately 35% greater than that of the pristine MnTe sample.

Acknowledgements

This work was supported by National Natural Science Foundation of China (Grant No. 51572098 and 51272080), National Basic Research Program of China (Grant No.2013CB632500), Natural Science Foundation of Hubei province (Grant No 2015CFB432), Open Fund of State Key Laboratory of Advanced Technology for Materials Synthesis and Processing, Wuhan University of Technology (No. 2016-KF-5). The technical assistance from the analytical and testing center of HUST is gratefully acknowledged.

References

[1] Snyder GJ, Toberer ES. Complex thermoelectric materials. Nat Mater 2008;7(2):105–14.
[2] Luo YB, Yang JY, Li G, Liu M, Xiao Y, Fu LW, et al. Enhancement of the thermoelectric performance of polycrystalline $In_4Se_{2.5}$ by copper intercalation and bromine substitution. Adv Energy Mater 2014;4(2):1300599.
[3] Zhao LD, Lo SH, Zhang YS, Sun H, Tan GJ, Uher C, et al. Ultralow thermal conductivity and high thermoelectric figure of merit in SnSe crystals. Nature 2014;508(7496):373–7.

[4] Xiao C, Li Z, Li K, Huang PC, Xie Y. Decoupling interrelated parameters for designing high performance thermoelectric materials. Accounts Chem Res 2014;47(4):1287−95.
[5] Guin SN, Chatterjee A, Negi DS, Datta R, Biswas K. High thermoelectric performance in tellurium free p-type $AgSbSe_2$. Energy Environ Sci 2013;6(9):2603−8.
[6] Tan GJ, Shi FY, Hao SQ, Chi H, Bailey TP, Zhao LD, et al. Valence band modification and high thermoelectric performance in SnTe heavily alloyed with MnTe. J Am Chem Soc 2015;137(35).
[7] Biswas K, He JQ, Zhang QC, Wang GY, Uher C, Dravid VP, et al. Strained endotaxial nanostructures with high thermoelectric figure of merit. Nat Chem 2011;3(2):160−6.
[8] Perumal S, Roychowdhury S, Negi DS, Datta R, Biswas K. High thermoelectric performance and enhanced mechanical stability of p-type $Ge_{1-x}Sb_xTe$. Chem Mater 2015;27(20):7171−8.
[9] Xiao Y, Yang JY, Jiang QH, Fu LW, Luo YB, Liu M, et al. A simultaneous increase in the ZT and the corresponding critical temperature of p-type $Bi_{0.4}Sb_{1.6}Te_3$ by a combined strategy of dual nano-inclusions and carrier engineering. J Mater Chem A 2014;2(47):20288−94.
[10] Heremans JP, Jovovic V, Toberer ES, Saramat Ail, Kurosaki K, Charoenphakdee A, et al. Enhancement of thermoelectric efficiency in PbTe by distortion of the electronic density of states. Science 2008;321(5888):554−7.
[11] Fu LW, Yang JY, Peng JY, Jiang QH, Xiao Y, Luo YB, et al. Enhancement of thermoelectric properties of Yb-filled skutterudites by an Ni-Induced "core−shell" structure. J Mater Chem A 2015;3(3):1010−6.
[12] Szuszkiewicz W, Dynowska E, Witkowska B, Hennion B. Spin-wave measurements on hexagonal MnTe of NiAs-type structure by inelastic neutron scattering. Phys Rev B 2006;73(10):104403.
[13] Cui JL, Li YP, Du ZL, Meng QS, Zhou H. Promising defect thermoelectric semiconductors $Cu_{1-x}GaSb_xTe_2$ (x=0−0.1) with the chalcopyrite structure. J Mater Chem A 2013;1(3):677−83.
[14] Allen JW, Lucovsky G, Mikkelsen JC. Optical properties and electronic structure of crossroads material MnTe. Solid State Commun 1977;24(5):367−70.
[15] Sato H, Tamura M, Happo N, Mihara T, Taniguchi M, Mizokawa T, et al. Electronic structure of NiAs-type MnTe studied by photoemission and inverse-photoemission spectroscopies. Solid State Commun 1994;92(11):921−4.
[16] Sato H, Tamura M, Happo N, Mihara T, Taniguchi M, Mizokawa T, et al. Electronic structure of NiAs-type MnTe. J Magnetism Magnetic Mater 1995;140:153−4.
[17] Iwanowski RJ, Heinonen MH, Witkowska B. X-ray photoelectron study of NiAs-type MnTe. J Alloys Compd 2010;491(1):13−7.
[18] Pei YZ, Wang H, Gibbs ZM, LaLonde AD, Snyder GJ. Thermopower enhancement in $Pb_{1-x}Mn_xTe$ alloys and its effect on thermoelectric efficiency. NPG Asia Mater 2012;4(9):e28.
[19] Lewis JE, Rodot H, Haen P. The low-temperature thermoelectric power and thermal conductivity of GeTe and of some GeTe-MnTe alloys. Phys Status Solidi 1968;29(2):743−54.
[20] Wu HJ, Chang C, Feng D, Xiao Y, Zhang X, Pei YL, et al. Synergistically optimized electrical and thermal transport properties of SnTe *via* alloying high-solubility MnTe. Energy & Environ Sci 2015;8(11):3298−312.
[21] Kim B, Kim I, Min B, Oh M, Park S, Lee H. Thermoelectric properties of non-stoichiometric MnTe compounds. Electron Mater Lett 2013;9(4):477−80.
[22] Youn SJ, Min BI, Freeman AJ. Crossroads electronic structure of MnS, MnSe, and MnTe. Phys Status Solidi 2004;241(7):1411−4.
[23] Xie WJ, Populoh S, Galazka K, Xiao XX, Sagarna L, Liu YF, et al. Thermoelectric study of crossroads material MnTe *via* sulfur doping. J Appl Phys 2014;115(10):103707.
[24] Sandratskii LM, Egorov RF, Berdyshev AA. Energy band structure and electronic properties of NiAs type compounds. II. Antiferromagnetic manganese telluride. Phys Status Solidi 2006;104(1):103−7.
[25] Zhao XB, Ji XH, Zhang YH, Zhu TJ, Tu JP, Zhang XB. Bismuth telluride nanotubes and the effects on the thermoelectric properties of nanotube-containing nanocomposites. Appl Phys Lett 2005;86(6):062111.

Yangyang Ren received his B.S degree from the School of Materials Science and Engineering, China University of Mining and Technology, PR China in 2014. He is currently a master degree candidate at the School of Materials Science and Engineering, Huazhong University of Science and Technology, PR China. His research interests are thermoelectric materials.

Qinghui Jiang is currently an associate professor in the School of Materials Science and Engineering at Huazhong University of Science and Technology, PR China. He obtained his Ph. D. degree from School of Materials Science and Engineering, Tsinghua University, PR China in 2007. He was a postdoctor at School of Engineering and Materials Science, Queen Mary University of London, UK (2011−2013). His research interests include thermoelectric materials, multiferroic materials, and ferroelectric material.

Junyou Yang is currently a professor and head of the Department of Materials Science, School of Materials Science and Engineering in Huazhong University of Science and Technology, PR China. He obtained his Ph. D. degree from Huazhong University of Science and Technology, PR China in 1996. He was a postdoctoral researcher at the Research Center of Advanced Science and Technology (RCAST), University of Tokyo, Japan (1999−2001). His research interests include thermoelectric materials, solar energy materials and solar cells.